na re

ARTICLES

PUBLISHED ONLINE: 27 NOVEMBER 2017 | DOI: 10.1038/NMAT5032

Chiral liquid crystal colloids

Ye Yuan[1†], Angel Martinez[1†], Bohdan Senyuk[1], Mykola Tasinkevych[2,3,4] and Ivan I. Smalyukh[1,5,6*]

Colloidal particles disturb the alignment of rmolecules into a non-chiral liquid crystal (LC) is that they induce chirality of the ensuing mes8–18

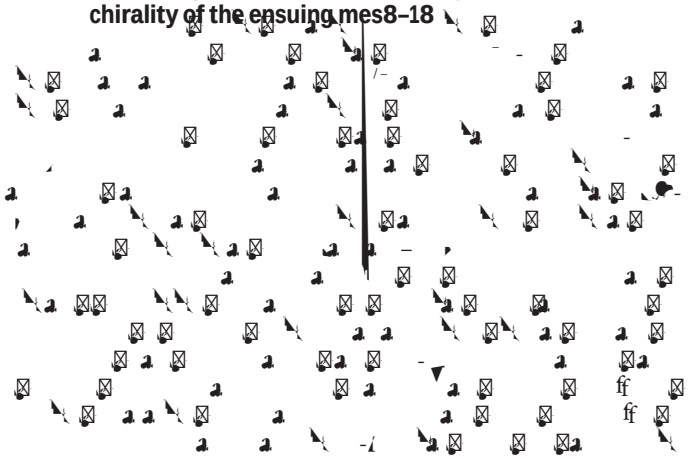

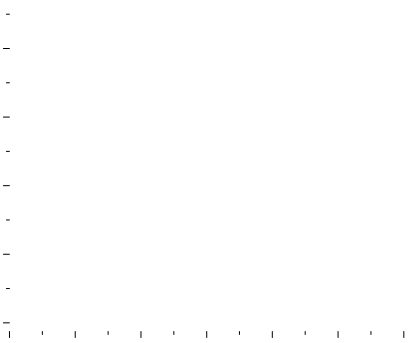

Figure 1 | Microsprings in a nematic liquid crystal. **a**,**b**, Right- and left-handed colloidal springs, respectively, imaged with the help of 3PEF-PM while surrounded by an isotropic medium (immersion oil). **c**,**d**, Self-diffusion of the particles oriented with the spring axis roughly parallel (**c**) or perpendicular (**d**) to n_0. The insets show optical bright-field micrographs at the corresponding orientations with respect to $\mathbf{n}_0$. Solid lines are Gaussian fits to experimental data allowing one to calculate diffusion coefficients[12] along and normal to n_0 (D_k D 2.9 10 ^{3} μm^2 s ^{1}, $D_?$ D 0.93 10 ^{3} μm^2 s ^{1} in **c** and D_k D 3.0 10 ^{3} μm^2 s ^{1}, $D_?$ D 2.7 10 ^{3} μm^2 s ^{1} in **d**). **e**–**j**, Optical micrographs of right- (**e**–**g**) and left-handed (**h**–**j**) colloidal microsprings in 5CB imaged using bright-field (**e**,**h**) and polarizing microscopy without (**f**,**i**) and with (**g**,**j**) an additional phase retardation plate (with the slow axis marked by the yellow double arrow) inserted between the crossed polarizers (white double arrows). **k**–**n**, Detailed analysis of **n**(**r**)-distortions induced in the LC by colloidal springs probed for the same particle using polarizing microscopy (**k**) and 3PEF-PM (**l**–**n**), with **l** and **n** showing details of two individual in-plane 3PEF-PM optical slices obtained for two different linear 3PEF-PM polarizations (marked by the green and red double arrows, respectively) and **m** showing the corresponding 3D perspective view of the particle reconstructed on the basis of superposition of many such slices. Scale bars are 5 μm.

Figure 2 | Chirality-dictated alignment of microsprings in a nematic liquid crystal. **a**, Orientation-dependent free energy cost of particle-induced elastic distortions versus the angle between the spring axis $\hat{\theta}_k$ (see **b**–**e** and Supplementary Fig. 1 for the definition of the orthonormal reference frame attached to the particle) and n_0 for different tilt directions of $\hat{\theta}_k$, and for the right- (circles) and left-handed (squares) particles. Open (solid) symbols correspond to the anticlockwise rotation of $\hat{\theta}_k$ about $\hat{\theta}_3(\hat{\theta}_?)$, as shown in –**e**. The insets depict free energy variations near the stable and metastable orientation states. **f**–**i**, Director structures around right-handed springs (**f**,**h**) at energy-minimizing orientations with D 4 (**f**) (blue solid circles in **a**) and with D 86 (**h**) (blue solid circles in **a**), and left-handed springs (**g**,**i**) with D 0 (**g**) (red open squares in **a**) and with D 90 (**i**) (red open squares in **a**) for the metastable (,**g**) and stable (**h**,**i**) particle orientations. **j**–**m**, Detailed director structures and defects corresponding to a colloidal spring shown in **g**. **n**– , Detailed director structures and defects corresponding to a spring shown in **i**. Director structures are shown with rods depicting local orientations of n(r) both at LC–particle interfaces and in the bulk, as well as with colour-coded patterns of azimuthal orientations of n(r) when projected from particle surfaces to the plane orthogonal to n_0, according to the colour scheme in the insets of **g** and **t**, as viewed from different perspectives.

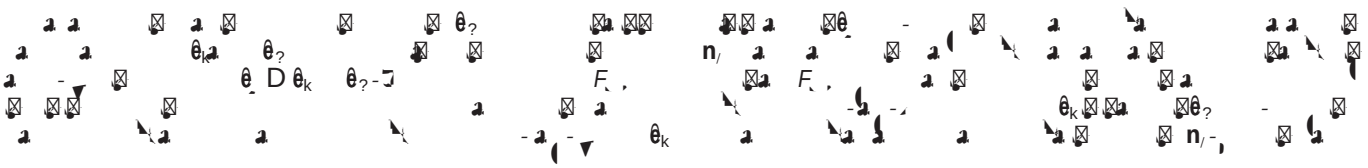

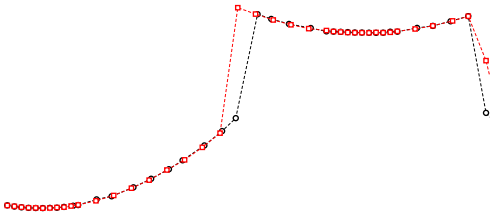

Figure 3 | Chirality-dictated alignment of single helices in a nematic liquid crystal. **a**–**f**, Optical micrographs of left-handed microhelices obtained using bright-field (**a**,**d**) and polarizing microscopy without (**b**,**e**) and with (**c**,**f**) a phase retardation plate. **g**,**h**, Self-diffusion of particles oriented with θ_k roughly orthogonal (**g**) and parallel (**h**) to n_0. The insets show optical bright-field micrographs at the corresponding orientations with respect to n_0 (D_k $D_?$ 2.2 10^{-3} $\mu m^2 s^{-1}$ in **g** and D_k 2.7 10^{-3} $\mu m^2 s^{-1}$, $D_?$ 0.68 10^{-3} $\mu m^2 s^{-1}$ in **h**). **i**, Orientation-dependent free energy cost of elastic distortions induced by particles versus the angle between θ_k and n_0 for different orientations of the tilt direction of θ_k, for left- (squares) and right-handed (circles) helices. Open (solid) symbols correspond to anticlockwise rotation of θ_k about $\theta_3(\theta_?)$, as shown in Fig. 2b–e. The insets depict free energy variations near the stable and metastable orientation states. **j**–**m**, Director structures around right-handed helices at D 8 (**j**) (blue solid circles in **i**) and at D 82 (**l**) (blue solid circles in **i**) and left-handed helices at D 0 (**k**) (red open squares in **i**) and at D 90 (**m**) (red open squares in **i**), which are stable (**j**,**k**) and metastable (**l**,**m**) particle orientations. The director field is shown with the help of rods and colour-coded azimuthal orientations of n(r) on particle surfaces relative to n_0 according to the colour scheme shown in the inset of **k**. Scale bars are 5 μm.

n r n /
F

Figure 4 | Chirality-dependent pair interactions of colloidal springs. **a**, Time-colour-coded trajectory of attraction of like-handed microsprings initially separated along n_0. The bottom inset shows colour scale of elapsed time counted from the moment of releasing particles from laser traps (t_{min}) until the moment when they approach each other at t_{max} (t_{max} t_{min} D 27 s), as shown in the bright-field micrographs in the inset. The final self-assembled colloidal structure for the same particles at t D 35 s > t_{max} is also shown in the inset in a slightly enlarged micrograph and emerges as a result of additional rotation of the colloidal springs around their axes. **b**, Separation distance d versus time corresponding to **a**, with the distance dependence of the corresponding interaction force shown in the inset. **c**, Time-colour-coded trajectory of repulsion of like-handed microsprings initially separated so that the separation vector is orthogonal to n_0. **d**, Time-colour-coded trajectory of repulsion of opposite-handed microsprings initially separated along n_0. The insets show the corresponding optical micrographs of the interacting particles. **e**, Separation distance versus time corresponding to **d**; the distance dependence of the corresponding interaction force is shown in the inset. **f**, Time-coded trajectory of attraction of opposite-handed microsprings initially separated so that the separation vector is orthogonal to n_0. The red curves in **b**,**e**, are the best fits of the experimental data with $d(t)$ D $(d_0^n$ n $t)^{1=n}$ where n D 5 for dipole–dipole interaction[21]; the fitting coe□cients are d_0 D 25 μm, D 1.3 10^5 μm^5 s ^{1} in **b** and d_0 D 29 μm, D 0.46 10^5 μm^5 s ^{1} in **e**. Solid red lines in the insets of **b** and **e** are the best linear fits with[21] ln F D $(n$ 1) ln d C const. Scale bars are 5 μm.

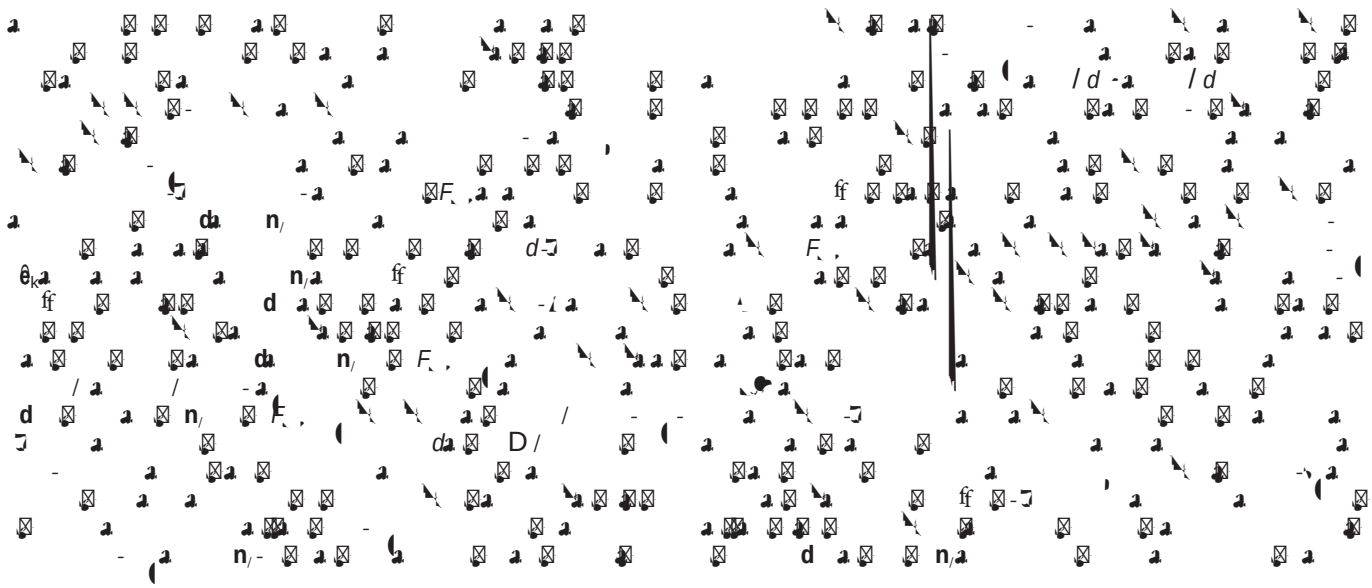

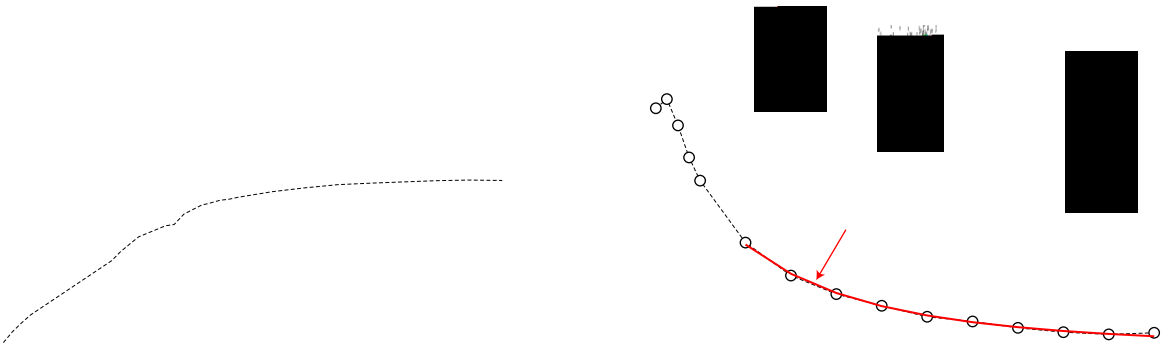

Figure 5

Figure 6 | Twisting of chiral particles relative to each other. **a**, Numerically calculated Landau–de Gennes free energy as a function of the angle $\varphi_\perp$ between the axes of like-handed springs, for the case when these spring axes rotate about the particles' $\hat{\theta}_\perp$ vectors in opposite directions and by equal amounts, as is shown schematically in **e**. The spring centre-to-centre vector **d** is fixed with $d = 1.625R$ and with the angle α between **d** and $\mathbf{n}_0$ at 90°. **b**, Free energy as a function of d at $\varphi_\perp = 180°$, all the other parameters are the same as in **a**. The insets in **a**,**b** show the director configurations around the springs with the help of rods and colour-coded azimuthal orientations, with respect to $\mathbf{n}_0$, of $\mathbf{n}(\mathbf{r})$ on particle surfaces. **c**,**d**, The case of like- (circles) and opposite-handed (squares) springs, depicting the free energy variations with $\varphi_\perp$ (particles' axes rotate about $\hat{\theta}_\perp$) or $\varphi_\parallel$ (particles' axes rotate about $\hat{\theta}_3$) at $d = 1.625R$ and $\alpha = 90°$, near the stable (**d**) and metastable (**c**) orientation states. Open (solid) symbols correspond to the case when the spring axes $\hat{\theta}_\parallel$ rotate about particles' aligned $\hat{\theta}_\perp$ vectors, see **e** ($\hat{\theta}_3$ vectors, see **f**) in opposite directions by equal amounts.

Conclusions

Methods